05

Upper Buffer Layer Influence on the Current-Carrying Capacity of Coated Conductors

© V.V. Guryev, V.E. Krylov, A.V. Irodova, O.A. Kondratiev, S.V. Shavkin

National Research Center „Kurchatov Institute“,
123182 Moscow, Russia
e-mail: Gurev_VV@nrcki.ru

Received May 6, 2025
Revised May 6, 2025
Accepted May 6, 2025

A systematic comparative analysis of the effect of the upper buffer layer on the transport characteristics of composite high-temperature superconducting tapes is performed. Two most common materials, cerium dioxide CeO_2 and lanthanum manganite $LaMnO_3$, are studied. It is shown that replacing CeO_2 with $LaMnO_3$ leads to an increase in the characteristic thickness of the superconducting layer, on which the critical current density drops by a factor of e, from 0.9 to 1.2 μm. When the external magnetic field is oriented in the plane of the tape, samples of both architectures showed the same critical current. When the field is oriented perpendicularly, samples with $LaMnO_3$ demonstrated higher critical currents, which indicates an increase in the concentration of pinning centers perpendicular to the tape plane. Due to the lack of self-epitaxy for $LaMnO_3$, it cannot completely replace CeO_2 on substrates with a moderate texture.

Keywords: current-carrying capacity, buffer layers, cerium dioxide, lanthanum manganite, anisotropic pinning model, cooperative potential well.

DOI: 10.61011/TP.2025.09.61927.83-25

Introduction

Discovery of high-temperature superconductivity [1] revolutionized a domain of technical superconductivity, which is aimed to producing strong magnetic fields. A key role here belongs to superconducting wires with a high current-carrying capacity and wires based high-temperature superconducting materials are beyond competition for many critical applications [2]. However, implementation of a potential of these materials encountered some serious technical difficulties. Its brittleness and complex crystal structure that results in anisotropy of properties were an essential obstacle for producing long-length wires.

The first generation of widely used high-temperature superconducting (HTSC) wires were wires based on oxides of bismuth, strontium, calcium and copper — BiSCCO. A technology of their manufacturing is based on standard metallurgical processes [3], as a result of which BiSCCO gets a pronounced texture required for maximizing the current-carrying capacity [4]. The most important disadvantage of the first-generation HTSC is a low irreversibility field. The superconducting state is preserved above it up to reaching an upper critical field, but the critical current is reduced up to the zero value. As a result, it is the irreversibility field, rather than the upper critical field, that determines boundaries of wire applicability. The low value of the irreversibility field and unsuccessful attempts to increase it resulted in rejection of further development of the technology of these wires.

In the second-generation HTSC (HTSC-2 also known as „composite HTSC tapes“ and „coated conductors“) based on $REBa_2Cu_3O_{7-\delta}$ (REBCO, RE is a rare earth element), the irreversibility field is much higher than for the first-generation wires [5].

In HTSC-2 mechanical strength is provided by a metal substrate tape, on which a heavily textured REBCO layer is applied. In order to prevent chemical interaction of the superconducting layer with the substrate [6], to match coefficients of thermal expansion and to create a high degree of texture, buffer layers are introduced [7]. Chemical interaction of REBCO with the environment at a substrate-opposite side is negated by a protective silver layer. An near-7 oxygen index $7-\delta$ required for superconductivity is obtained by annealing in oxygen at the temperatures 400 °C–450 °C. The final manufacturing stages includes application of a shunt copper layer to the wire, which contributes to stable operation of the wire. An architecture of the resultant composite tape is a real masterpiece of high technologies: the metal carrying tape of the thickness of 30–100 μm, one to six buffer layers with the thicknesses from 20 to 2500 nm, the superconducting layer from 0.5 to 3 μm, the protective silver layer of about 5 μm and the shunt copper layers of 5–40 μm at each side of the tape. At the same time, the nanometer thicknesses of the buffer layers are kept at kilometer lengths.

The composite HTSC tapes demonstrated excellent operating characteristics — the high current-carrying capacity at acceptable mechanical properties, which provides a hope for their wide application in many fields [2]. As of today, many companies worldwide already propose them as products, thereby indicating a successfully-tested „proof-of-concept“

stage and readiness of the technology for introduction into the industry.

Among the components of the composite tape, the buffer layers are one of the critical elements that determine a quality and characteristics of the entire tape [8]. In addition to the mentioned technological functions, they also determine a microstructure of the superconducting layer. In particular, grain orientation, a defect density and the quality of the crystal structure of the superconducting layer directly depend on the upper buffer layer in contact with it [9]. Thus, optimization of the buffer layers is a key trend in developing the high-performance composite HTSC tapes [10].

The present study is focused on comparative analysis of the two most commercially-popular upper buffer layers — cerium dioxide CeO_2 and lanthanum manganite $LaMnO_3$ (LMO). Both the compounds are studied quite well. Cerium dioxide is widely applied in various industries, including chemical-mechanical polishing, ore purification, biomedicine and other fields as well [11]. It has a cubic fluorite structure and unusual magnetic properties [12]. LMO perovskite manganite was thoroughly studied due to its extremely demanded properties, such as colossal magnetoresistance under pressure and formation of fully-spin-polarized conduction bands [13]. At the temperatures below 140 K it is an antiferromagnetic insulator with an orthorhombic structure, while at the temperatures above 750 K it transits into a pseudocubic ferromagnetic metal [13].

For the technology of HTSC-2 manufacturing, interest to CeO_2 and LMO is caused by their chemical stability at the typical REBCO growth temperatures [14] and good consistency of the structural parameters with the REBCO parameters, while mismatch is below 1 %, which is necessary for epitaxial growth. In case of CeO_2 the mismatch is negative (the buffer parameter is less than the typical parameters for REBCO), while for LMO it is positive. Despite a noticeable number of the studies dedicated to investigation of [15,16] and CeO_2 [17,18] as the buffer layers, comparative studies of the influence of these materials on the current-carrying capacity of the composite HTSC tapes are very limited. It is due to a multifactorial nature of the technological process and accompanying complexity of controlled variation of only one of the factors, in this case is a material of the upper buffer layer. Nevertheless, taking into account colossal importance of these studies for further development of the technology, they are of considerable interest. When the „clean“ experiment is impossible, comparison of the results obtained in several independent studies can minimize the influence of random and incompletely controlled factors.

1. Experiment and methods

1.1. Samples

The samples of the composite HTSC tape based on YBCO ($YBa_2Cu_3O_{7-\delta}$) were manufactured in an experimental technological line in NRC „Kurchatov Institute“ [19–21]. The basic technology consists of 7 successive stages.

1. Preparation of a surface of the tape from AISI 310 steel of the thickness of0.1 mm and the width of 4 mm, which includes mechanical polishing, ultrasonic cleaning and optical control of a surface quality.

2. Application of the basic buffer layer of yttrium-stabilized zirconium dioxide (YSZ) to the tape by means of ion-beam dissipation and formation of a texture in it using an assisting ion etching beam in the ABAD machine(Alternating Beam-Assisted Deposition). The dissipated target consists of a metal alloy of zirconium and yttrium, while the YSZ oxide layer is formed due to dissipation in the oxygen medium. The texture is formed due to a difference of the ion etching rates along various crystallographic directions. The YSZ layer with the required texture is formed when the assisting ion beam is directed at the angle of 35° to the tape plane. In order to obtain a required sharpness of the texture, $\Delta\varphi \approx 9°$, the thickness of the YSZ layer shall exceed 1 μm. In the basic technology, it is about 2 μm. The method of forming the texture by means of assisting ion etching is a standard of the modern technology for HTSC-2.

3. Application of the additional CeO_2 buffer layer by means of Pulsed Laser Deposition (PLD). A laser radiation source is an excimer laser designed to operate on the XeCl gas mixture, with the wavelength of 308 nm. The parameters of growth of CeO_2: the substrate heater temperature is 750 °C, the oxygen pressure is 1 mTorr, the laser radiation energy is 600 mJ, the pulse repetition rate is 200 Hz, the tape movement speed is 42 m/h and the number of passes through a growth area is 4. These parameters provide formation of the CeO_2 layer of the thickness of about 150 nm and the texture sharpness $\Delta\varphi \leq 7°$.

4. Application of the YBCO layer by means of PLD. The targets with the different densities and the various chemical composition are used. Optimal conditions of YBCO growth are searched for each target. The growth parameters used in the present study: the temperature of the heater of the substrate with the buffer layers is 975 °C, the oxygen pressure is 100 mTorr, the laser radiation energy is 650 mJ, the passes is 200 Hz and the tape movement speed is 36 m/h. The thickness of the YBCO layer varies by changing the number of passes through a growth chamber. In the present study, the number of passes was 9, 19 and 27, which corresponded to the following thicknesses of the YBCO layer: 0.5, 0.95 and 1.2 μm.

5. Application of the protective silver layer by thermal sputtering. In order to provide adhesion of silver to the YBCO surface, prior to application, the surface is activated by glow-discharge plasma in the oxygen medium using a cathode electrode. The thickness of the produced layer is about 5 μm.

6. The composite tape is annealed in oxygen at the pressure of 850 mbar and the temperature of 450 °C for 4 h.

7. Galvanic application of a stabilizing copper coating at each side of the tape, which has a thickness of about 20 μm.

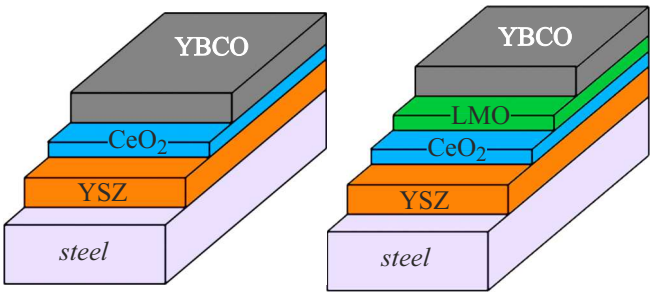

Figure 1. Diagrams of the architectures of the composite HTSC tapes (the layers of silver and copper are not shown). The basic architecture obtained in the technological line in „Kurchatov Institute“ is shown on the left. The modified architecture with the additional LMO layer is shown on the right.

Each technological stage, except for 3 and 4, where the same PLD machine is applied, is carried out in specialized equipment, therefore, a transition from one stage to another is accompanied by extracting the samples into atmospheric conditions.

The output of the presented technological process gives out the composite HTSC tape of the thickness of about 0.15 mm, with the architecture shown on Fig. 1 on the left.

The preliminary experiments showed that LMO has no self-epitaxy effect [22] and when is directly applied to the YSZ layer, the texture sharpness is completely inherited from this layer without improvement. Since for eliminating weak intergranular bonds in the YBCO layer a substrate (buffer) texture sharpness threshold is about 7° [23], the architecture of the YSZ/LMO buffer layers is not considered here.

In order to study the LMO buffer layer, we have used the YSZ/CeO_2/LMO architecture with the CeO_2 intermediate layer (Fig. 1, on the right), and for this purpose an operation of application of the LMO layer was added into the basic technology between the stages 3 and 4. The parameters of growth of this layer: the temperature of the heater of the YSZ/CeO substrate is$_2$ 800 °C, the oxygen pressure is 150 mTorr, the laser radiation energy is 500 mJ, the pulse repetition rate is 200 Hz, the tape movement speed is 42 m/h and the number of passes through the growth area is 4.

1.2. Experimental procedures

The structural characteristics of the superconducting and buffer layers were studied by X-ray diffraction at the room temperature in the four-circle diffractometer Rigaku SmartLab using monochromatic Cu$K_{\alpha 1}$-radiation and the beam 0.4×2 mm (the sizes are in a diffraction plane and perpendicular to it). The standard $\theta-2\theta$ diffraction patterns (2θ is within the range $5-80°$) from the tape plane were used. The texture sharpness $\Delta\varphi$ was evaluated by reflections {111} for CeO_2 and {103} for YBCO, which are obtained by rotating the samples around the normal to the tape surface; in both the cases $\Delta\varphi$ was determined an average half-width of reflections, while an error was determined as a standard deviation from the average.

The thicknesses of the superconducting and buffer layers were measured in the scanning electron-ion microscope Helios NanoLab 600i in sample transects produced by ion etching.

The critical current was determined using the criterion of 1 μV/cm that is achieved in the current-voltage curves (CVC) during standard transport measurements in the four-contact method. The angular dependences of the critical current $I_c(\theta)$ were measured in the so-called maximum Lorentz force configuration, when the magnetic field is perpendicular to the transport current. The angle θ was quantified relative to the tape plane. The angular dependences were studied in liquid nitrogen (77.4 K) at the atmospheric pressure in an external magnetic field of up to 1.5 T.

1.3. Methodology of analysis of the angular dependences of the critical current

A method of analysis of the angular dependences of the critical current has been previously proposed by us [24,25]. Taking into account its novelty and that it is still not a common tool, it is advisable to shortly present main provisions here. The method is based on an Anisotropic Pinning Model (APM) that uses a concept of a cooperative potential well. This potential well is formed by cooperative action of all the pinning centers within a physically small volume of vortex matter [26]. Thus, the APM considers not individual pinning of separate vortices, but pinning of a certain representative volume of a vortex substance — a vortex assembly. Without the transport current, the vortex assembly occupies the most favorable position at a bottom of the cooperative well, wherein a minimum of specific energy of the magnetic flux does not assume that each vortex captured by the nearest pinning centers is at the bottom of its own individual potential well. Under effect of the transport current, the vortex assembly rises up a slope of the cooperative potential well along the Lorentz force. If the Lorentz force exceeds a maximum steepness of the slope of this well, then all the vortex matter is moved, thereby resulting in emergence of an electric field and energy dissipation. A volume pinning force can be expressed as:

$$F_p = -\max\left(\frac{\delta U}{\delta L}\right) = -\frac{U_0(\boldsymbol{B})}{L_0(\boldsymbol{j}, B)}, \qquad (1)$$

where U and L — the depth and the width of the cooperative potential well, $L_0 = U_0/\max(\delta U/\delta L)$ — the effective geometrical size (width) of the cooperative potential well, U_0 — the effective depth of the cooperative potential well.

The model postulates that the effective depth of the cooperative potential well $U_0(\boldsymbol{B})$ depends on a value of magnetic induction and its direction only, rather than the Lorentz force. On the contrary, the width of the cooperative

potential well $L_0(\boldsymbol{j}, B)$ is determined by an absolute value of magnetic induction (a vortex density) and the Lorentz force. Thus, it takes into account a dual nature of anisotropy: not only with respect to the direction of the magnetic field, but with respect to the direction of the Lorentz force. The effective width of the cooperative well L_0 is determined by a minimum distance between two energy-equivalent positions of the vortex assembly. This distance can be roughly evaluated by assuming a minimum of the two values: an average intervortex distance or a typical distance between adjacent (along a direction of possible motion) pinning centers.

All specific features of superconductor pinning are determined by the angular dependences of the depth of the cooperative well U_0 and its size L_0. Based on a large number of complementary experiments [25–30], it was shown that both for the superconducting Nb–Ti-tape and for HTSC-2 [25] the angular dependences U_0 and L_0 were described by ellipsoids:

$$\left(\frac{\cos(\alpha)}{U_x}\right)^2 + \left(\frac{\cos(\beta)}{U_y}\right)^2 + \left(\frac{\cos(\gamma)}{U_z}\right)^2 = \frac{1}{U_0^2}, \quad (2a)$$

where $\cos(\alpha)$, $\cos(\beta)$, $\cos(\gamma)$ — the direction cosines of an induction vector, U_x, U_y, U_z — the semi-axes of the energy ellipsoid.

Similarly for the size body

$$\left(\frac{\cos(\alpha')}{L_{x'}}\right)^2 + \left(\frac{\cos(\beta')}{L_{y'}}\right)^2 + \left(\frac{\cos(\gamma')}{L_{z'}}\right)^2 = \frac{1}{L_0^2}, \quad (2b)$$

where $\cos(\alpha')$, $\cos(\beta')$, $\cos(\gamma')$ — the direction cosines of the vector of the Lorentz force, $L_{x'}$, $L_{y'}$, $L_{z'}$ — the semi-axes of the size ellipsoid.

In accordance with a basic postulate of the model (1), in order to determine a critical value of the pinning force at pre-defined conditions, it is necessary to divide a value of the energy ellipsoid (along the induction vector) by a value of the size ellipsoid (along the Lorentz force).

For the experiment geometry that corresponds to measurement of the angular dependences of the critical current, this model results in the following dependence [25]:

$$I_c(\theta) = I_c^0 \sqrt{\frac{[k^L \cos\theta]^2 + [\sin\theta]^2}{[k^U \cos(\theta-\theta_0)]^2 + [\sin(\theta-\theta_0)]^2}}. \quad (3)$$

Here, I_c^0, k^L, k^U, θ_0 are fitting parameters with the following physical meaning: I_c^0 — the scale multiplier that has the dimension of current; $k^U = U_y/U_z$ and $k^L = L_{z'}/L_{y'} = L_N/L_T$ — the ratio of the semi-axes of the energy ellipsoid and the size ellipsoid, which for the size ellipsoid coincide with the transverse direction (T) and the normal direction (N) of the composite HTSC tape [25]. The parameter θ_0 is responsible for a degree of asymmetry of the angular dependences and characterizes an angle of relative revolution of the energy ellipsoid $U(\theta)$ and the size ellipsoid $L(\theta)$ [25]. A microscopic cause of origin of a non-zero angle θ_0 is deviation of a lattice plane ab from the tape plane [25], which is often observed in the tapes, in which the texture is produced by means of the assisting ion beam [31].

When the parameter $\theta_0 \approx 0$, the critical current I_c coincides with the scale multiplier I_c^0 with orientation of the magnetic field in the tape plane ($\theta = 0^\circ$). By a definition, $I_c(\theta = 0^\circ)$ is pre-defined by a pinning force (1), directly proportional to the depth of the cooperative well in the transverse direction U_T (as per the direction of the magnetic field) and reversely proportional to the width of the cooperative well in the direction of the normal L_N (as per the direction of the Lorentz force): $I_c(\theta = 0^\circ) \sim F_p(0^\circ) = U_T/L_N$. Similarly, $I_c(90^\circ) \sim U_N/L_T$. This implies that with the angles θ_0 close to zero, $I_c(0^\circ)/I_c(90^\circ) \approx k^U/k^L$.

2. Experimental results

Fig. 2 shows the images of the cross section of the composite HTSC tapes (Fig. 1), which are obtained in the scanning electron microscope. The thickness of the CeO_2 buffer layer is about $0.15\,\mu$m for all the samples, while the thickness of the LMO layer in the modified architecture is about $0.04\,\mu$m. The YBCO thicknesses vary from 0.5 to $1.2\,\mu$m and are approximately the same for the paired (of the same thickness of the YBCO) samples of both the architectures under consideration.

Table 1 shows X-ray data for both the architectures. The texture sharpness for the YBCO layer is below 6°. The content of oxygen in YBCO, which is evaluated by a ratio of intensities of reflections (005) and (006), according to [32], is the highest, $\delta \approx 0$ in $YBa_2Cu_3O_{7-\delta}$. The value of $\Delta_{mis} = (a_{buf} - a_{av})/a_{buf}$ that characterizes mismatch of the parameter of the upper buffer layer a_{buf} with the average parameter of YBCO $a_{av} = (a + b)/2$ is below 1 %.

Fig. 3 shows the dependence of the critical current on the thickness of the YBCO layer. It is known that with increase of the thickness of the superconducting layer the critical current reaches saturation, which is related to origin of the a-phase, whose crystallographic axis c is oriented in the tape plane [33]. At the same time, probability of origin of the a-phase is affected by mismatch Δ_{mis} of the parameters of the superconducting layer and a layer on which it is applied [34], i.e. the material of the upper buffer layer. It is clear in Fig. 3 that with the same thickness of the YBCO layer the critical current for the CeO_2/LMO/YBCO modified architecture shows higher values than for the CeO_2/YBCO basic architecture and this difference increases with increase of the thickness of the YBCO. At the same time, the texture in the YBCO layer for the modified architecture is worse than for the basic one (the width of reflections $\Delta\varphi\,\{103\}$ is higher (Table 1)).

Fig. 4 compares the angular dependences of the critical current in the fields 0.1, 0.3 and 1 T. With orientation of the field within the tape plane, the critical currents of the samples with both the architectures are almost identical. Anisotropy of the critical current is noticeably reduced

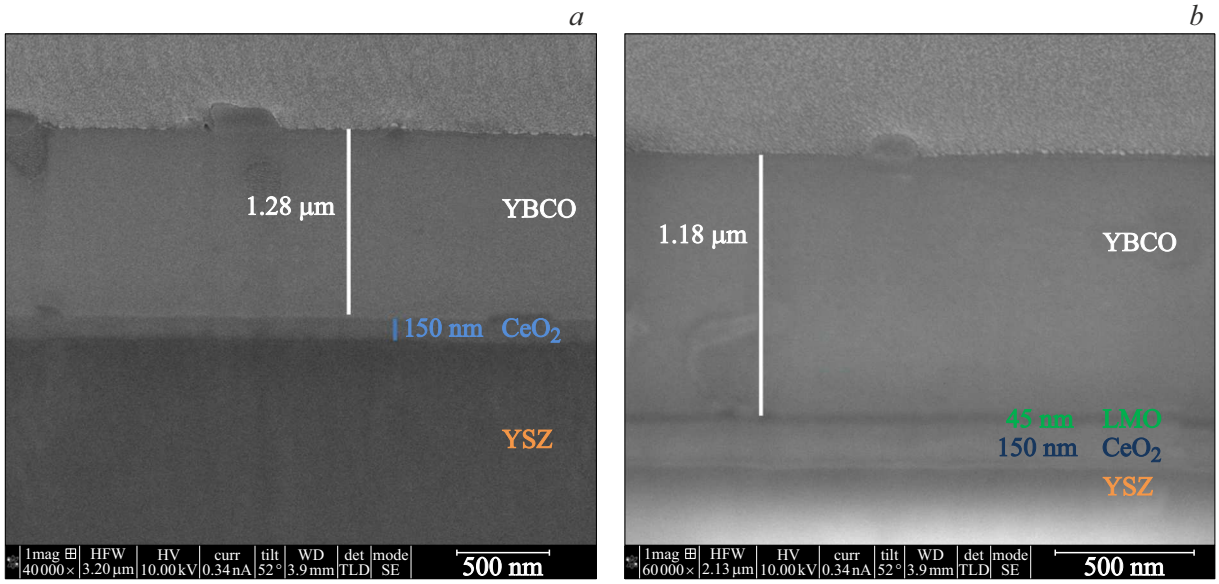

Figure 2. SEM images of a cross section of the samples with the architectures YSZ/CeO_2/YBCO (*a*) and YSZ/CeO_2/LMO/YBCO (*b*).

Table 1. Structural characteristics for the architectures CeO_2/YBCO and CeO_2/LMO/YBCO

	CeO_2/YBCO	CeO_2/LMO/YBCO
YBCO $\Delta\varphi\{103\}$ (°)	4.2 ± 0.5	5.1 ± 0.5
CeO_2 $\Delta\varphi\{111\}$ (°)	5.8 ± 0.3	7.0 ± 0.3
I (005)/I (006)	0.61	0.64
Δ_{mis}	−0.5 %	0.8 %

in the modified architecture, with the LMO upper buffer layer: a current ratio in the two extreme orientations $I_c(\theta = 0°)/I_c(\theta = 90°)$ is less than in the basic architecture approximately by 15 % Besides, the sample with the LMO buffer layer exhibits a weak smeared peak in the fields 0.3 and 1 T. Such an effect is usually related to a system of long defects that penetrate the entire thickness of the YBCO layer and act as the pinning centers [35,36]. For the CeO_2/YBCO basic architecture, such a pronounced peak is not observed with orientation of the field along the normal to the tape.

In case of equality of the critical currents, the anisotropy reduced as compared to the basic architecture is preserved for all the values of the field within the range from 0.1 to 1.5 T with orientation of the field in the tape plane (Fig. 5).

Among the studies that investigated the influence of the upper buffer layer on the current-carrying capacity of the HTSC [34,37], only one can be found, which directly compared LMO and CeO_2 as the upper buffer layers [38]. As in our case, in the study [38], decrease of anisotropy of the critical current of the YBCO was observed (when using the target without the artificial pinning centers) when replacing CeO_2 with LMO. We note that in the study [38] the basic buffer layer was IBAD-MgO

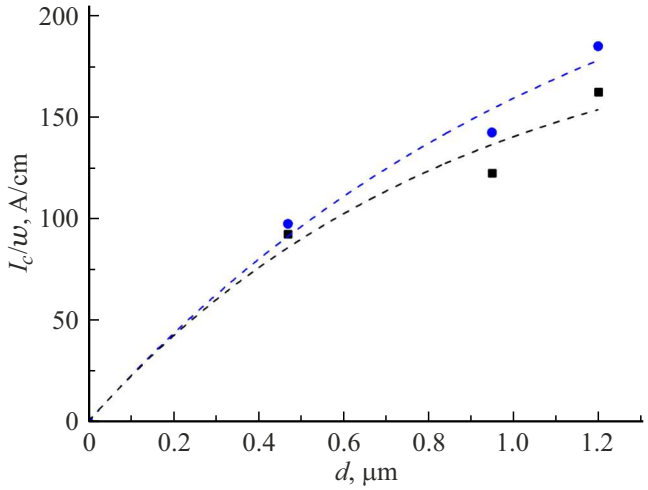

Figure 3. Dependence of the critical current in the intrinsic magnetic field on the thickness of the YBCO layer (the dots). The black squares correspond to the CeO_2/YBCO basic architecture, while the blue circles correspond to the CeO_2/LMO/YBCO modified architecture. The lines mark an exponential approximation in accordance with the formula (4) (see Section 3).

(Ion Beam Assisted Deposition), which is fundamentally different from our ABAD-YSZ. This circumstance can indicate independence of the obtained results on the used technology.

3. Discussion

In order to evaluate a typical thickness, at which the density of the critical current decreases in e times, we approximated the data of Fig. 3 with an exponential

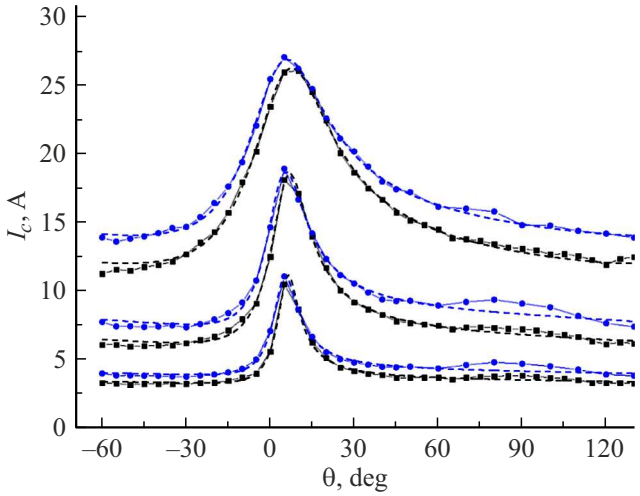

Figure 4. Angular dependences of the critical current for the samples of the two architectures with the YBCO layer's thickness of 0.45 μm in the fields 0.1, 0.3 and 1 T (from top to bottom). The angle $\theta = 0°$ corresponds to orientation of the field in the tape plane, while the angle $\theta = 90°$ corresponds to orientation of the field along the normal to the tape. The black squares mean the CeO_2/YBCO basic architecture, the blue circles mean the CeO_2/LMO/YBCO architecture and the dashed lines mean approximation according to (3).

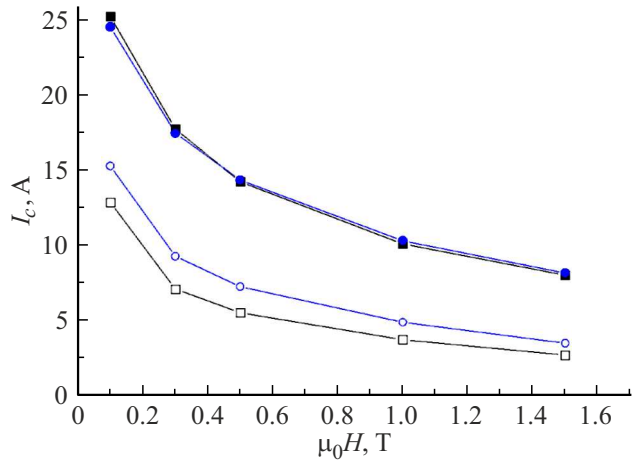

Figure 5. Field dependences of the critical current at the nitrogen temperature in the perpendicular field (the open symbols) and in the field in the tape plane (the close symbols) for the CeO_2/YBCO basic architecture (the black color) and the CeO_2/LMO/YBCO modified architecture (the blue color).

dependence:

$$I_c(d) = I^{sat}\{1 - \exp(-d/d_0)\}, \qquad (4)$$

where I^{sat} and d_0 are fitting parameters which have a meaning of the current in a large-thickness limit and a typical thickness of decrease of the current density, respectively. The estimated values of the parameter d_0 were 1.2 and 0.87 μm, while those of the parameterI^{sat} were 282 and 206 A for the architectures CeO_2/LMO/YBCO and CeO_2/YBCO, respectively. The dependence (4) means exponential reduction of the density of the critical current from a certain initial value $j_c(0) = I^{sat}/(wd_0)$ to zero in the large-thickness limit [33]. It is noteworthy that the found values of I^{sat} and d_0 result in the same value of the critical current density in the small-thickness limit for both the architectures: $j_c(0) = 2.37 \cdot 10^6$ A/cm^2.

We note that the method of analysis of the angular dependences of the critical current, which is described in Section 1.3, does not take into account a smeared peak with orientation of the field along the normal to the tape plane, which is observed in the CeO_2/LMO/YBCO architecture. However, as can be concluded from comparison of the approximation (3) and the experimental data (Fig. 4), it does not noticeably contribute to the total angular dependence and can be regarded as a small correction.

Table 2. Fitting parameters in the formula (3) for the two architectures of the HTSC tape and the average intervortex distance a (see explanations in the text)

Magnetic field, T	a, nm	CeO_2/YBCO				CeO_2/LMO/YBCO			
		I_c^0	θ_0	k^L	k^U	I_c^0	θ_0	k^L	k^U
0.1	144	24.5	11.2	1.85	3.56	25.1	7.5	2.17	3.53
0.3	83	16.9	6.9	3.16	8.06	17.1	5.5	3.82	7.87
0.5	64	14.0	5.5	4.05	11.11	14.1	4.6	4.56	10.3
1	45	10.4	3.8	5.01	15.03	10.2	3.4	5.08	12.81
1.5	37	8.0	3.3	4.75	14.96	8.0	3.0	4.72	12.90

Table 2 shows the fitting parameters from the formula (3) for the fields from 0.1 to 1.5 T for the considered architectures of the HTSC tape. One should note several trends as well as proximity of the values of some parameters (underlined in Table 2)

There is stable trend of decrease of the value of θ_0 when increasing the magnetic field from 0.1 to 1.5 T: from 11.2 to 3.3° for the CeO_2/YBCO architecture and from 7.5 to 3.0° for the CeO_2/LMO/YBCO architecture, thereby reflecting the degree of asymmetry of the angular dependences. The decrease of θ_0 can be interpreted as manifestation of a growing role of collective effects in the vortex system, when the energy profile begins to be defined to a larger extent by interaction between the vortices, rather than their association with the pinning centers only.

As noted above, the critical currents with orientation of the field in the tape plane $I_c(0°)$ are similar for the two architectures in all the studied fields, which is reflected in proximity of the respective parameters I_c^0. This implies the equality $U_T^{\mathrm{LMO}}/L_N^{\mathrm{LMO}} = U_T^{\mathrm{CeO}}/L_N^{\mathrm{CeO}}$, at least, at small θ_0, i.e. in the quite high fields. Here, the indices LMO and CeO correspond to the architectures CeO_2/LMO/YBCO and CeO_2/YBCO. However, taking into account that the YBCO layers are produced with dissipation of the same

target and at the same mode, we assume that the stronger equalities are fulfilled: $U_T^{\mathrm{LMO}} = U_T^{\mathrm{CeO}}$, $L_N^{\mathrm{LMO}} = L_N^{\mathrm{CeO}}$.

The external field determines an average intervortex distance (Table 2), which can be evaluated as $a \approx \sqrt{(\Phi_0/B)}$, where Φ_0 is a quantum of the magnetic flux, B is induction of the external field. In the small field, 0.1 T, when intervortex interaction is small, the parameters k_{CeO}^U and k_{LMO}^U are almost the same, while k_{CeO}^L and k_{LMO}^L significantly differ. Thus, the bond energy of the vortex assembly with the pinning-center system is the same for both the architectures, while the typical distance between the two energy-equivalent positions is different. Taking into account the equalities $U_T^{\mathrm{LMO}} = U_T^{\mathrm{CeO}}$ and $L_N^{\mathrm{LMO}} = L_N^{\mathrm{CeO}}$, it can be concluded that there are pinning centers that are elongated along the normal and a typical distance between them in the transverse direction is significantly smaller for the CeO_2/LMO/YBCO architecture than for the CeO_2/YBCO architecture: $L_T^{\mathrm{LMO}} < L_T^{\mathrm{CeO}}$. This interpretation is in qualitative agreement with the previously mentioned explanation of the smeared peak near 90° [35,36]. It follows from the definition of k^L in the formula (3) and the values of Table 2 that $L_T^{\mathrm{CeO}} = L_T^{\mathrm{LMO}}(k_{\mathrm{LMO}}^L/k_{\mathrm{CeO}}^L) = 1.17L_T^{\mathrm{LMO}}$, i.e. L_T^{CeO} exceeds L_T^{LMO} approximately by 17 %.

With increase of the field from 0.5 to 1 T, the intervortex distance decreases from 64 to 45 nm and the situation is changed to the opposite: the parameters k_{CeO}^L and k_{LMO}^L are close, while k_{CeO}^U and k_{LMO}^U differ. With further increase of the field from 1 to 1.5 T, the parameters k_{CeO}^U and k_{LMO}^U remain almost unchanged, while the parameters k_{CeO}^L and k_{LMO}^L decrease. It can be interpreted as a decrease of the intervortex distance to the values that are less than the typical distance between the pinning centers in the transverse direction. This interpretation allows estimating as follows: $45\,\mathrm{nm}\,(0.5\,\mathrm{T}) < L_T^{\mathrm{LMO}} < 64\,\mathrm{nm}\,(1\,\mathrm{T})$.

Based on the obtained value of L_T^{LMO} and the data about the parameter k_{LMO}^L in Table 2, it is possible to evaluate the width of the cooperative well along the normal L_N^{LMO} from 100 to 330 nm. This estimate exceeds the intervortex distance almost for all the studied fields and looks overestimated. However, it should be taken into account that with orientation of the magnetic field in the tape plane and a thickness of the YBCO, which is several intervortex distances, the influence of the edge effects (barriers for input and output of vortices at the boundaries YBCO/Ag and YBCO/the upper buffer) is great and the width of the cooperative well can not be evaluated using the intervortex distance and the typical distance between the pinning centers (see Section 1.3).

Conclusion

We have comparatively analyzed the current-carrying capacity of the composite HTSC tapes of the two architectures — with the upper buffer layer made of cerium dioxide CeO_2 and the layer made of lanthanum manganite $LaMnO_3$. The experimental results demonstrate the advantage of $LaMnO_3$ in the following aspects:

1) noticeable increase of the typical thickness of the superconducting layer, at which the density of the critical current is reduced — from 0.9 μm for CeO_2 to 1.2 μm for $LaMnO_3$;

2) significant reduction of anisotropy of the critical current at the level of 15 % with close values of the critical current in the magnetic field oriented in the tape plane.

However, one should note a fundamental limitation in application of $LaMnO_3$, which is related to no self-epitaxy effect, thereby making it impossible to use it on the substrates of a moderate texture sharpness, $\Delta\varphi > 7°$, and requiring preservation of the CeO_2 intermediate layer.

Based on analysis within the framework of the anisotropic pinning model, it is concluded that there is the increase of the concentration of the pinning centers with predominant orientation along the normal to the tape plane for the architecture with the $LaMnO_3$ upper buffer layer. The distance between the energy-equivalent positions of the vortex assembly in the transverse direction is 45–64 nm for $LaMnO_3$ and 52–77 nm for CeO_2.

Acknowledgments

The X-ray measurements were carried out in equipment of the Kurchatov Complex for Sychrotron and Neutron Research. The microscopic studies are carried out in equipment of the Resource Center for Probe and Electron Microscopy.

Funding

This study was carried out under the state assignment of the National Research Center „Kurchatov Institute“.

Conflict of interest

The authors declare that they have no conflict of interest.

References

[1] J.G. Bednorz, K.A. Müller. Z. Physik B — Condensed Matter., **64**, 189 (1986). https://doi.org/10.1007/BF01303701
[2] J.L. MacManus-Driscoll, S.C. Wimbush. Nature Rev. Mater., **6**, 587 (2021). https://doi.org/10.1038/s41578-021-00290-3
[3] K. Heine, J. Tenbrink, M. Thöner. Appl. Phys. Lett., **55**, 23 (1989). https://doi.org/10.1063/1.102295
[4] T.D. Aksenova, P.V. Bratukhin, S.V. Shavkin, V.L. Melnikov, E.V. Antipova, N.E. Khlebova, A.K. Shikov. Physica C, **205** 3–4 (1993). https://doi.org/10.1016/0921-4534(93)90392-4
[5] A. Gurevich. Nature Mater., **10**, 255 (2011). https://doi.org/10.1038/nmat2991
[6] N.A. Moshchalkova. V sb.: *Obzory po vysokotemperaturnoi sverkhprovodimosti,* pod red. T.Yu. Maslennikova (MTsNTI, M. 1990), v. 1 (in Russian).

[7] B. Holzapfel, J. Wiesmann. In: *Handbook of superconductivity,* ed. by A. Gardwell, C. Larbalestier, I Braginski (CRC Press, 2023), v. II.
[8] J.M. Phillips. J. Appl. Phys., **79**, 1829 (1996). https://doi.org/10.1063/1.362675
[9] S.R. Foltyn, P.N. Arendt, Q.X. Jia, J.L. MacManus-Driscoll, L. Stan, Y. Li, X. Zhang, P.C. Dowden. J. Mater. Research., **19**, 6 (2011). https://doi.org/10.1557/JMR.2004.0244
[10] M.T. Paulose, J.S. Sandra, M.A. Sayeed, V. Selvamanickam. IEEE Trans Appl. Supercond., **35**, 5 (2025). https://doi.org/10.1109/TASC.2024.3513942
[11] T. Montini, M. Melchionna, M. Monai, P. Fornasiero. Chem. Rev., **116** (2016). https://doi.org/10.1021/acs.chemrev.5b00603
[12] K. Ackland, J.M.D. Coey. Phys. Reports, **746**, 1 (2018). https://doi.org/10.1016/j.physrep.2018.04.002
[13] P. Rivero, V. Meunier, W. Shelton. Phys. Rev. B, **93**, 024111 (2016). https://doi.org/10.1103/PhysRevB.93.024111
[14] W. Wong-Ng, Z. Yang, G. Liu, Q. Huang, L.P. Cook, S. Diwanji, C. Lucas, M.-H. Jang, J.A. Kaduk. In: *Advances and Applications in Electroceramics,* ed. by K.M. Nair. et al. (Wiley, 2011)
[15] F. Fan, Y. Lu, Z. Liu, D. Zhou, Y. Guo, C. Bai, M. Li, C. Cai. Supercond. Sci. Technol., **33**, 055003 (2020). https://doi.org/10.1088/1361-6668/ab7c51
[16] K. Venkataraman, E. Hellstrom. J. Mater. Res., **24**, 4 (2009). https://doi.org/10.1557/JMR.2009.0180
[17] S. Dong-Qi, M. Ping, K. Rock-Kil, K. Ho-Sup, C. Jun-Ki, S. Kyu-Jeong, P. Chan. Chin. Phys. Soc., **16**, 7 (2007). https://doi.org/10.1088/1009-1963/16/7/058
[18] A.V. Boryakov, D.V. Masterov, S.A. Pavlov, A.E. Parafin, P.A. Yunin. FTT, **66**, 6 (2024) (in Russian). DOI: 10.61011/FTT.2024.06.58235.20HH
[19] V.V. Gur'ev, I.V. Kulikov, I.M. Abdyukhanov, M.V. Alekseev, Yu.N. Belotelova, P.V. Volkov, P.V. Konovalov, V.S. Kruglov, V.E. Krylov, D.V. Lazarev, A.A. Nikonov, A.V. Ovcharov, D.N. Rakov, S.V. Shavkin. FTT, **65**, 12 (2023). http://dx.doi.org/10.61011/FTT.2023.12.56725.5015k (in Russian).
[20] V.V. Gur'ev, V.E. Krylov, I.V. Kulikov, I.M. Abdyukhanov, M.V. Alekseev, Yu.N. Belotelova, P.V. Konovalov, P.A. Luk'yanov, M.V. Mal'tseva, S.N. Nikolaev, S.V. Shavkin. FTT, **12** (2024). http://journals.ioffe.ru/articles/59565 (in Russian).
[21] A.V. Irodova, I.D. Karpov, V.S. Kruglov, V.E. Krylov, S.V. Shavkin, V.T. Em. ZhTF. **91**, 12 (2021). http://dx.doi.org/10.21883/JTF.2021.12.51761.169-21 (in Russian).
[22] T. Taneda, M. Yoshizumi, T. Takahashi, R. Kuriki, T. Shinozaki, T. Izumi, Y. Shiohara, Y. Iijima, T. Saitoh, R. Yoshida, T. Kato, T. Hirayama, T. Kiss. IEEE Trans. Appl. Supercond., **3** (2013). https://doi.org/10.1109/TASC.2012.2235113
[23] H. Hilgenkamp, J. Mannhart. Rev. Modern Phys., **74** (2002). https://doi.org/10.1103/RevModPhys.74.485
[24] V. Guryev, S. Shavkin, V. Kruglov. J. Phys.: Conf. Ser., **2103** (2021). https://doi.org/10.1088/1742-6596/2103/1/012096
[25] V.V. Gur'ev, S.V. Shavkin, I.V. Kulikov. VANT: seriya termoyadernyi sintez, **47**, 3 (2024) (in Russian). DOI: 10.21517/0202-3822-2024-47-3-93-107
[26] E.Yu. Klimenko, S.V. Shavkin, P.V. Volkov. J. Exp. Theor. Phys., **85**, 3 (1997). https://doi.org/10.1134/1.558341
[27] S. Shavkin,V. Guryev, V. Kruglov, A. Ovcharov, I. Likhachev, A. Vasiliev, A. Veligzhanin, Y. Zubavichus. EPJ Web Conf., **182** (2018). doi.org/10.1051/epjconf/201818508007
[28] V.V. Guryev, S.V. Shavkin, V.S. Kruglov. Physica C, **599**, 1354080 (2022). https://doi.org/10.1016/j.physc.2022.1354080
[29] V.V. Guryev, S.V. Shavkin, V.S. Kruglov. J. Phys.: Conf. Ser., **1697** (2020). doi.org/10.1088/1742-6596/1697/1/012202
[30] V.V. Guryev, A.V. Irodova, N.K. Chumakov, S.V. Shavkin. St. Petersburg State Polytechnical University J. Phys. Mathemat., **16**, 1.1 (2023). https://doi.org/10.18721/JPM.161.111
[31] J. Lee, J. Bang, G. Bradford, D. Abraimov, E. Bosque, D. Larbalestier. IEEE Trans. Appl. Supercond., **35**, 5 (2025). https://doi.org/10.1109/TASC.2024.3505115
[32] J. Ye, K. Nakamura. Phys. Rev. B, **48**, 10 (1993). https://doi.org/10.1103/PhysRevB.48.7554
[33] G. Majkic. In: *Superconductivity. From Materials Science to Practical Applications,* ed. by Mele (Springer, 2020)
[34] A.E. Shchukin, A.R. Kaul'. Inorg Mater., **58** (2022). https://doi.org/10.1134/S0020168522130015
[35] Z.L. Wang, D.H. Lowndes, D.K. Christen, D.M. Kroeger, C.E. Klabunde, D.P. Norton. Physica C, **252**, 1–2 (1995). https://doi.org/10.1016/0921-4534(95)00428-9
[36] Y.V. Cherpak, V.A. Komashko, S.A. Pozigun, A.V. Semenov, C.G. Tretiatchenko, E.A. Pashitski, V.M. Pan. IEEE Trans. Appl. Supercond., **15**, 2 (2005). https://doi.org/10.1109/TASC.2005.848212
[37] T.G. Holesinger, S.R. Foltyn, P.N. Arendt, Q. Jia, P.C. Dowden, R.F. DePaula, J.R. Groves. IEEE Trans. Appl. Supercond., **11**, 1 (2001). https://doi.org/10.1109/77.919783
[38] M.Z. Khan, E. Rivasto, Y. Wu, Y. Zhao, C. Chen, J. Zhu, H. Palonen, J. Tikkanen, H. Huhtinen, P. Paturi. J. Phys.: Conf. Ser., **1559** (2020). https://doi.org/10.1088/1742-6596/1559/1/012037

Translated by M.Shevelev